Materials Science & Engineering A 638 (2015) 165–173

Contents lists available at ScienceDirect

Materials Science & Engineering A

journal homepage: www.elsevier.com/locate/msea

Foam behavior of solid glass spheres – Zn22Al2Cu composites under compression stresses

J.A. Aragon-Lezama [a,*], A. Garcia-Borquez [b], G. Torres-Villaseñor [c]

[a] Departamento de Materiales, Universidad Autónoma Metropolitana-A, Avenida San Pablo 180, Colonia Reynosa Tamaulipas, 02200 México, D.F., México
[b] Ciencia de Materiales, ESFM – Instituto Politécnico Nacional, Edif. 9, Unid. Prof. A. Lopez Mateos, Colonia Lindavista, 07738 México, D.F., México
[c] Departamento de Metálicos y Cerámicos, Instituto de Investigaciones en Materiales, Universidad Nacional Autónoma de México, Apdo., P 70-360, México, D.F., México

ARTICLE INFO

Article history:
Received 10 December 2014
Received in revised form
17 April 2015
Accepted 19 April 2015
Available online 30 April 2015

Keywords:
Foam
Composite
Microstructure characterization
Scanning electron microscopy
Compression

ABSTRACT

Solid glass spheres – Zn22Al2Cu composites, having different densities and microstructures, were elaborated and studied under compression. Their elaboration process involves alloy melting, spheres submersion into the liquid alloy and finally air cooling. The achieved composites with densities 2.6884, 2.7936 and 3.1219 g/cm^3 were studied in casting and thermally induced, fine-grain matrix microstructures. Test samples of the composites were compressed at a 10^{-3} s^{-1} strain rate, and their microstructure characterized before and after compression by using optical and scanning electron microscopes. Although they exhibit different compression behavior depending on their density and microstructure, all of them show an elastic region at low strains, reach their maximum stress (σ_{max}) at hundreds of MPa before the stress fall or collapse up to a lowest yield point (LYP), followed by an important plastic deformation at nearly constant stress (σ_p): beyond this plateau, an extra deformation can be limitedly reached only by a significant stress increase. This behavior under compression stresses is similar to that reported for metal foams, being the composites with fine microstructure which nearest behave to metal foams under this pattern. Nevertheless, the relative values of the elastic modulus, and maximum and plateau stresses do not follow the Ashby equations by changing the relative density. Generally, the studied composites behave as foams under compression, except for their peculiar parameters values (σ_{max}, LYP, and σ_p).

1. Introduction

Alloys rich in Zn have been investigated extensively in recent years [1–7]. It is well know that Zn, as a pure element, has very limited properties for industrial applications, whereas Al-based alloys like Zn22Al, Zn27Al and Zn4.6Al with small quantities of Cu, Mg or Ag have attracted the researchers attention because their surprising superplastic property [8–12], when they have a fine-grained microstructure and are deformed under a quasi-static rate. Basic studies are also of interest, because of the strong dependence between microstructure and properties, varying, for example, the type and/or quantities of alloying elements, or the elaboration process like thermal, mechanical, or thermo-mechanical [13–17]. For example, ZnAlCu alloys are normally synthesized by the conventional casting process because it is easy, fast and economical; however the resulting microstructure presents some defects that limit its application under compression.

On the other hand, Zn22Al and Zn27Al alloys have found further applications as foams (or sponges) and composites. In general, this kind of materials can exhibit attractive properties [18–20], for example, high mechanical resistance at low density, super-plasticity, etc. Moreover, metal matrix composites have good wear resistance and as metallic foams or sponges are good energy absorbers. Some metal matrix composites (MMC) based on Zn22Al alloy have been synthesized with several structural components like whiskers or particles of SiC [21–25], Al_2O_3 [26], ZnO [27], graphite [28], hydroxyapatite [29] and $CuZn_5$, $CuZn_2$, $CuAl_2$ [30]. Interesting here is the reported mechanical behavior under compression or tensile stresses, applied at different strain rates to evaluate super-plasticity or damping conducts by measuring internal friction. All these new properties make them very interesting for engineering applications.

Hitherto, metallic foams based on Zn22Al alloy have been prepared by different procedures. For example, the eutectoid composition Zn22Al alloy was produced as foam, using the melt foaming method with $CaCO_3$ [31,32] or titanium hydride (TiH_2) [33] as blowing agent, and adding short Al_2O_3 fibers [34] or SiC [35,36] as reinforcement and

* Corresponding author. Tel.: +52 55 53189475.
E-mail addresses: alja@correo.azc.uam.mx (J.A. Aragon-Lezama), a.garciaborquez@yahoo.com.mx (A. Garcia-Borquez), gtorres@unam.mx (G. Torres-Villaseñor).

http://dx.doi.org/10.1016/j.msea.2015.04.048
0921-5093/

stabilizing agents. Also, foams of Zn22Al with open-cells [37] and Zn22Al–1Cu having different microstructures [38], induced by heat treatment, have been elaborated by a replication process of NaCl preforms to study the compressive behavior and energy absorption capacity. The first work on closed-cells Zn–22Al foams elaborated by the powder metallurgy technique was also performed corroborating its strain rate sensitivity [39]. Moreover, a novel Zn22Al syntactic foam composite was reached via stir casting (vortex), with different volume fractions (6–50 vol%) of Ni-coated fly ash micro-balloons as foaming agent. The effect of the fly ash volume fraction on the microstructure, compressive behavior and sensitivity to the strain rate were determined [40].

No research has been reported before about the preparation and characterization of composites based on Zn22Al eutectoid alloy, having solid glass spheres as the structural component. Therefore, it would be interesting to study their mechanical behavior under compression in order to improve this property.

In this work it is reported the microstructural characterization and compressive behavior of an original composite with three different densities, formed by solid glass spheres in Zn22Al2Cu matrix alloy with two different microstructures. One of them, the original casting microstructure with its well-known structural defects, and the other one, the thermally induced fine microstructure, with superplastic property. At this point, it is interesting to study the influence of the glass spheres, as structural component, in the mechanical properties of both kind of microstructure in matrix.

The composites were prepared by an innovative method and tested under compressive stresses at a quasi-static strain rate. They behave in general like solid foams. Their compression behavior changes with the matrix microstructure and the composite density, but they do not follow the Ashby equations for the foams. However, they reach higher maximum stresses by lower densities than conventional foams or syntactic foams with similar matrixes.

2. Background

2.1. Composites

The density of a composite can be calculated from the densities and volume fractions of its individual components according to the mixtures rule equation:

$$\rho_c = \rho_s X_s + \rho_m X_m \quad (1)$$

where ρ is the density, c the composite, s the structural component, m the matrix, and X the volume fraction.

It is known that the elastic modulus (E) of any particulate composite lies between two limit values, named upper, E_{UL}, and lower, E_{LL}, limits. They can be calculated by the following equations:

$$E_{UL} = X_s E_s + (1 - X_s) E_m \quad (2)$$

$$E_{LL} = 1/[X_s/E_s + (1 - X_s)/E_m] \quad (3)$$

Eqs. (2) and (3) are the direct and inverse mixture rules inferred for elastic modulus of long fibers composites with strain applied towards a parallel and perpendicular direction with respect to the fibers, respectively [19].

2.2. Foams

Relative elastic modulus of foams to matrix, E_f/E_m, has been reported [41] to follow a quadratic or cubic behavior with respect to the corresponding relative densities, ρ_f/ρ_m, as long as the foams have open or closed cells, correspondingly:

$$E_f/E_m = C_1(\rho_f/\rho_m)^a \quad (4)$$

Here C_1 is a constant, $a=2$ for open cells and $a=3$ for closed cells.

Similarly, it has been found that the collapse stress and plateau stress of foams relative to yield stress of matrix, σ_{col}/σ_{ym} and σ_p/σ_{ym}, respectively, vary with the relative density, ρ_c /ρ_m, according to the Ashby equations [41]:

$$\sigma_{col}/\sigma_{ym},\ \sigma_p/\sigma_{ym} = C_2(\rho_c/\rho_m)^{3/2} \quad (5)$$

Here C_2 is a constant.

3. Material and methods

3.1. Alloy preparation

99.99% Zn, 99.27% Al and 99.999% Cu ingots were employed to prepare Zn22Al2Cu alloy by conventional casting in a crucible introduced in a muffle furnace previously heated at 700 °C. The mass of each component was measured using a precision balance (10^{-4} g), Mettler H45. The alloy density was determined by Archimedes method as 5.4 g/cm^3.

3.2. Composites elaboration

The raw materials used in this work were Zn22Al2Cu (Zinalco) alloy and solid spheres of borosilicate glass. Mariefeld manufacturing spheres of 4 mm diameter were selected with the following characteristics: melting point at 1100 °C, Young modulus between 78 and 85 GPa, density of 2.5 g/cm^3 and a chemical composition of 61–67% SiO_2, 10–18% Na_2O, 5–10% CaO, 3–8% Al_2O_3, 1–5% B_2O_3 and 0.5–3% MgO.

Composites elaboration was carried out using a three steps process: first, melting the alloy at 700 °C and heating the solid glass spheres at 400 °C, separately; second, introducing the preheated spheres into the molten alloy; third, slowly cooling the mixture in air. Flotation of spheres was avoided by pushing them with a cylindrical bar until the mixture viscosity was enough to retain them during the cooling. Fig. 1 shows the resulting glass spheres distribution into the matrix alloy.

To obtain composites of different densities, a constant alloy mass of 890 g was employed with 243.3, 300 and 400 g of structural component.

3.3. Density determination

A mass/volume ratio method was used to determine the composites density. For that, samples in parallelepiped form of

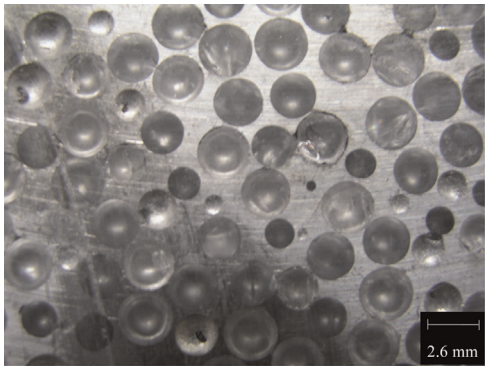

Fig. 1. Optical image showing the solid glass spheres distribution into the matrix alloy, forming the composite. In this case with density of 2.6884 g/cm^3.

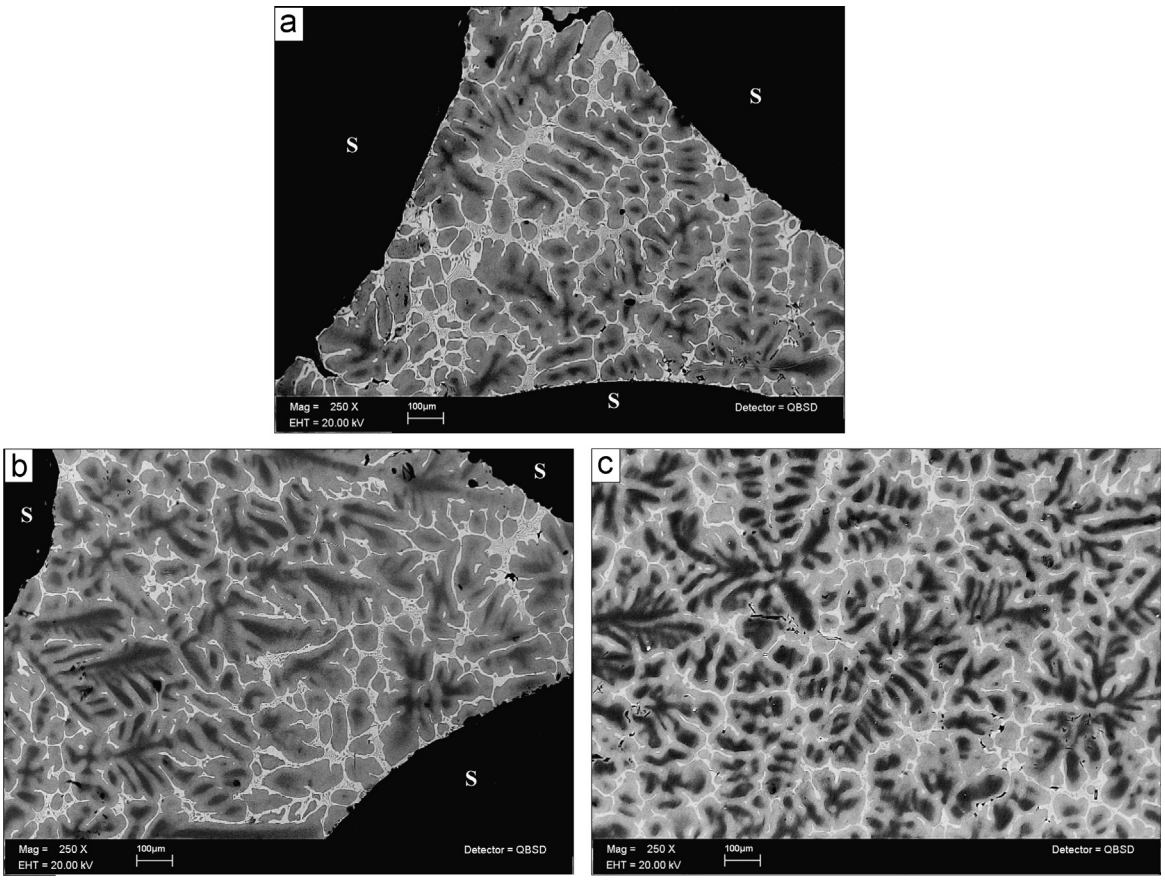

Fig. 2. BSE–SEM-image showing the casting microstructure of composites with different densities: (a) 2.6884, (b) 2.7936 and (c) 3.1219 g/cm^3. S: sphere.

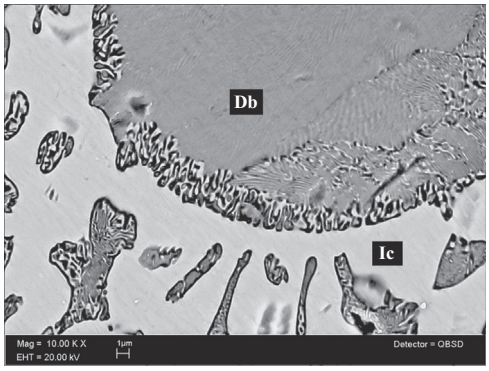

Fig. 3. Dendritic branch (Db) and interdendritic component (Ic) details in the casting microstructure showing the fine nanostructure of Al (dark) – Zn (clear) alternated phases. BSE–SEM-image.

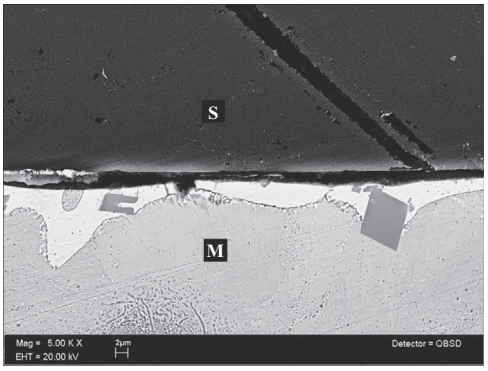

Fig. 4. BSE–SEM-image showing thin layer rich in Zn (clear contrast) formed at the matrix (M) border around the spheres (S). There is also a slight separation between sphere and matrix.

$0.8 \times 0.8 \times 1.6$ cm^3 were cut by using a tungsten carbide disk. The length of each side was measured with an accuracy of 10^{-3} cm and the corresponding volume was determined. The respective mass was obtained with 10^{-4} g accuracy using a Mettler H45 balance.

The three composites average densities obtained were 2.6884, 2.7936 and 3.1219 g/cm^3.

3.4. Matrix microstructures

The casting microstructure in matrix was obtained during the composite elaboration, i.e., by non-equilibrium cooling from 700 °C to room temperature in air.

A second microstructure in matrix was thermally induced thereafter by maintaining the composites with a casting microstructure at 350 °C during 45.5 h, followed by quenching in acetone at 0 °C. This microstructure will be named as a thermally induced microstructure.

3.5. Metallographic preparation

In order to reveal the microstructure, samples were finely polished using diamond paste and thereafter etched with 1% HNO_3 in C_2H_6O. The microstructure was analyzed by optical and scanning electron microscopies, using Olympus PMG3 and Leica Cambridge instruments, respectively.

3.6. Compressive tests

Samples $0.8 \times 0.8 \times 1.6\ cm^3$ of the solid Zn22Al2Cu alloy and the elaborated composites were tested in a universal Instron machine under compression at a $10^{-3}\ s^{-1}$ strain rate. The composites samples were photographed with an Olympus digital camera, before (Fig. 1) and after (Figs. 15 and 16) the compression tests.

4. Results

4.1. Casting microstructure

It is quite evident from Fig. 2 that the casting microstructure changes with the composite density, i.e., with the spheres volumetric fraction. The typical microstructure having dendritic and interdendritic components can be observed in the matrix of the three composites. Dendritic branches (Db) have Al-rich dark centers, fenced by a Zn–Al solid solution having a gray tonality. The interdendritic component is distinguished by its clear nuance. Both components exhibit a fine nanostructure formed by two alternated phases, as shown in Fig. 3, and again the interpretation of the z-contrast of the back-scattered electrons, identifies the Al (dark) and Zn (clear) phases. Dendritic occupancy was observed to increase with the composite density.

It is interesting to remark that always a Zn-enrichment was observed in the matrix surfaces in contact with the spheres. This effect could possibly be due to a thermal gradient between both materials, since they have very different heat capacities. Moreover, matrix and spheres were slightly separated, as viewed in Fig. 4, because of the matrix thermal contraction during the cooling process.

4.2. Thermally induced microstructure

Fig. 5 shows the thermally induced microstructure having nearly homogeneous microstructure with a few Zn (clear contrast) and Al (black contrast) islands. The large homogeneous microstructure is constituted by a fine substructure of alternated Zn or Al sheets having a thickness of 200 nm, see Fig. 6a. Near the spheres the grains grew up

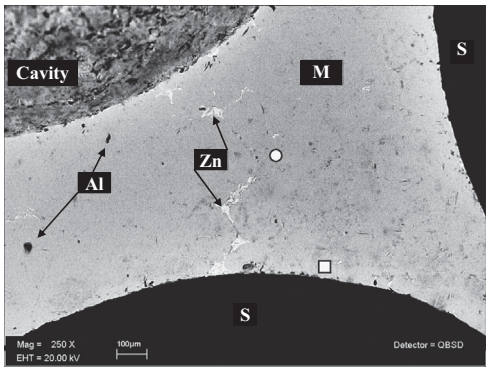

Fig. 5. BSE–SEM-image of a thermally induced fine microstructure representative in matrix. S: sphere, and M: matrix. Composite with density of 2.7936 g/cm^3. See also Fig. 6.

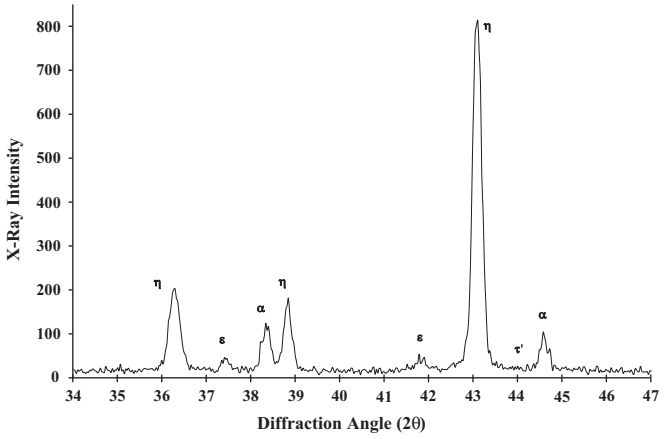

Fig. 7. Characteristic X-ray diffraction pattern of the elaborated Zn22Al2Cu alloy.

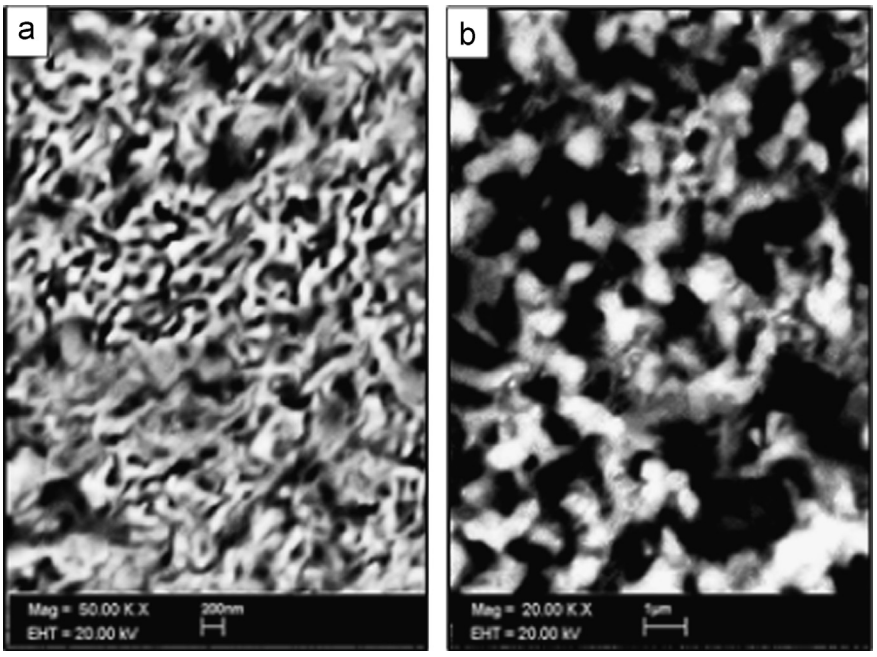

Fig. 6. Detail of the homogeneous part at fine microstructure in Fig. 5. (a) Alternated 100–200 nm thick Zn–Al sheets (circle in Fig. 5) and (b) ~1 μm grains at the matrix in contact with the spheres (square in Fig. 5).

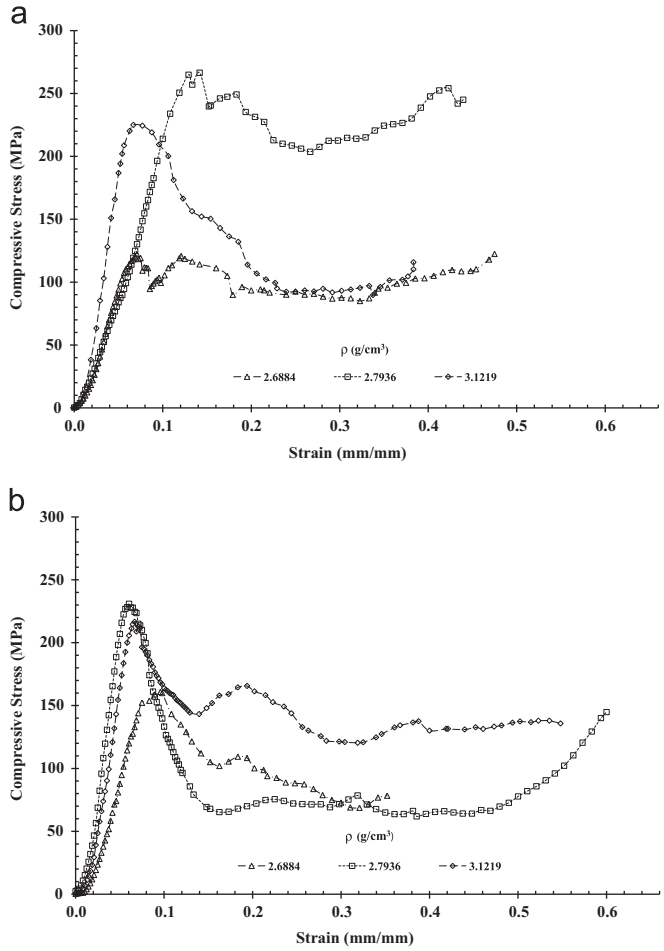

Fig. 8. Compressive stress–strain curves of composites with three different density values: (a) casting matrix microstructure and (b) fine matrix microstructure.

Table 1
Composites densities (ρ_c) and sphere volume fractions (X_s)

ρ_c (g/cm^3)	Volume fraction (X_s)
2.6884	0.9350
2.7936	0.8987
3.1219	0.7855

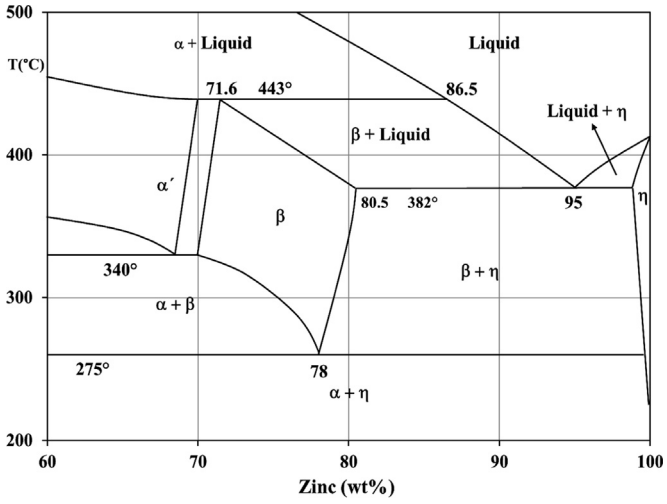

Fig. 9. Zn-rich side of the Zn–Al phase diagram [45].

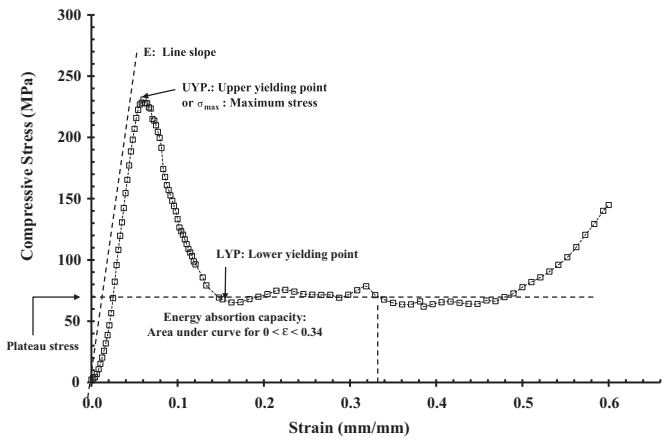

Fig. 10. Compressive stress–strain curve of the composite with 2.7936 g/cm^3, defining important parameters as well as behavior regions discussed in this work.

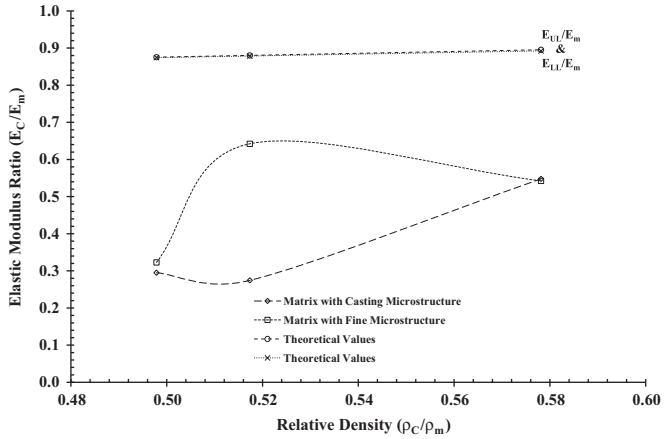

Fig. 11. Graph showing the dependence of the elastic modules ratio on the relative density for the composites with casting and fine microstructures and theoretical limits that belong to elastic modules ratio of composites.

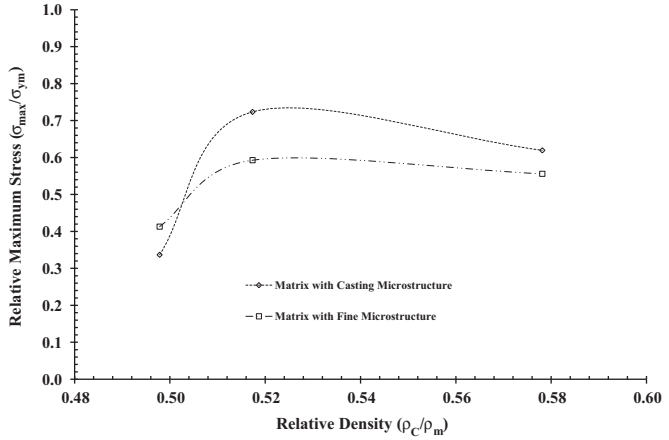

Fig. 12. Graph of the relative maximum stress as a function of the relative density for the composites with casting and fine microstructures in matrix.

to 1 μm mean size, Fig. 6b. Such microstructures will be referred as a thermally induced microstructure or simply a fine microstructure.

Characteristic X-ray diffraction pattern of this microstructure is shown in Fig. 7. It has the typical phases corresponding to the alloy Zn22Al2Cu as reported by different works [42–44]. α and η are Al-rich and Zn-rich equilibrium phases, respectively, and ε is the $CuZn_4$ intermetallic phase.

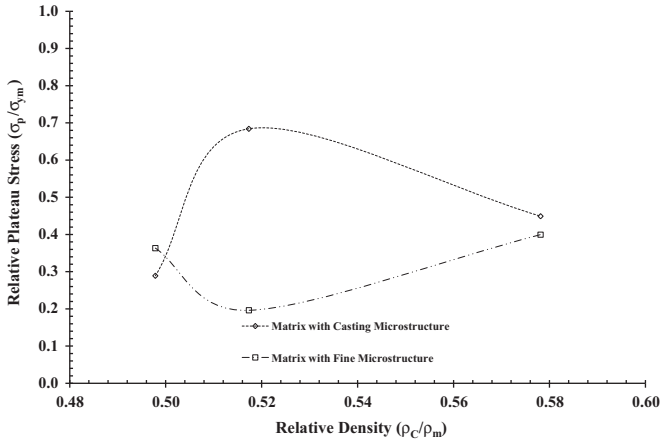

Fig. 13. Graph of the dependence of the relative plateau stress on the relative density of the composites with casting and fine microstructures in matrix.

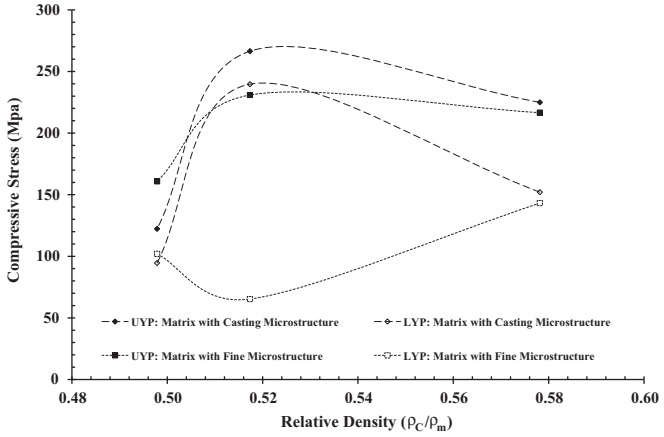

Fig. 14. Graph of the upper and lower yielding points, UYP and LYP, as a function of relative density.

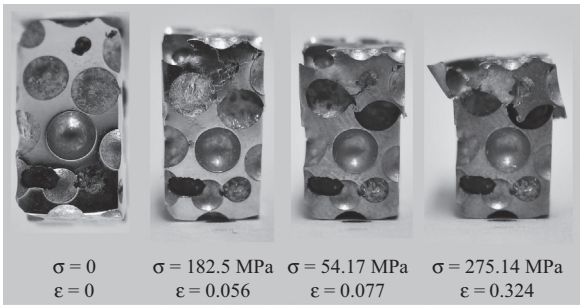

Fig. 15. Representative optical image of composite sample with casting microstructure deformed stage by stage. In this case with density of 2.6884 g/cm^3.

During the quenching some spheres pieces split from the matrix, leaving tiny bits of glass adhered to it, whose appearance suggests that a local micro-fusion took place. The bad thermal dissipation of the glass spheres conduces to retention of heat in the matrix, and this explains why the microstructure near them had bigger grains.

4.3. Compression tests

The solid Zn22Al2Cu alloy tested under compression had a Young modulus of about 90 GPa, regardless the microstructure in matrix, and yield stress of 363 MPa and 390 MPa for the casting and fine microstructures, respectively.

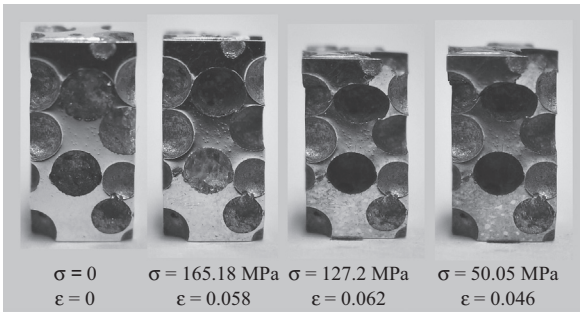

Fig. 16. Representative optical image of composite sample with fine microstructure deformed stage by stage. In this case with density of 2.6884 g/cm^3.

Compressive stress–strain curves of the composites with casting and thermally induced microstructures are shown in Fig. 8, referring the corresponding densities. In general, the curves show three different behaviors. Nearby relative low strains (<0.1), the stress increases linearly. After reaching a maximum value, the stress decreases until a fluctuating value, defining a plateau stress region by increasing strain. Finally, most composites required a continuous increasing of stress to get additional and higher deformations.

5. Discussion

5.1. Density and its effect

Densities measured in the elaborated composites were nearly half of the Zinalco alloy density and lower than the lowest density reported for a similar Zn22Al syntactic foam (3.3 g/cm^3), containing 50 vol% microballoons [40], and the density measured for an hybrid material of a Zinalco alloy with 20 mass% of Al_2O_3 (3.83 g/cm^3) [26].

Using the three composites density values (ρ_c) obtained in the mixtures rule Eq. (1) in Section 2.1, it was calculated the corresponding volume fraction of spheres (X_s) in the composites, see Table 1. Note that $X_m+X_s=1$. The obtained component vol% values are higher than those reported for the Zn22Al syntactic foams mentioned before [40].

5.2. Microstructure contrast and phases

Considering the atomic number of the alloy elements and the different effect they have on the electrons backscattering (BSE) power, it was possible to distinguish the alloy components by using SEM z-contrast images. Then the darkness at the dendritic branches centers means they were rich in Al, because it is the lightest element with the lowest electrons backscattering power producing the lowest contrast, i.e., the dark tonality. On the other hand, the clear tonality corresponding to the highest contrast is produced by elements having the highest electrons backscattering power, which in turn means the heaviest element in the alloy with the highest z-value, i.e., the element Zn. All this means that the interdendritic component that exhibits alternated clear and dark sheets is formed by Zn and Al-rich phases, respectively. Compositional analysis by EDXS on each component confirmed these facts.

The two-phase-alternated substructures are known as pearlite type constituent and are formed in interdendritic component and dendritic branches by eutectic and eutectoid transformations, respectively.

Likewise, regions fenced by cooling in non-equilibrium conditions are formed in the casting microstructure through a peritectic

transformation at 71.6 wt% Zn and 443 °C, according to the Zn–Al phase diagram, Fig. 9.

The fraction of fenced Al-rich dark dendrites centers increases with increasing density, at the expense of the interdendritic component whose fraction decreases. That means that the net fluence of Al atoms taking place from the Al-rich dendrite nucleus, through the fence, to interdendritic regions, increases with the decreasing composite density, i.e., with higher spheres volumetric fraction. This behavior can be explained as an effect caused by the low thermal conductivity of the glass spheres, delaying the heat dissipation from the matrix, when they are close to each other, and thus giving more time for the Al atoms diffusion.

The microstructure in the matrix attached to the spheres, fine grains of 1 μm size, is very similar to that obtained in the Zn22Al2Cu alloy, after solution annealing for 1 h at 350 °C and quenching in ice water at 15 °C [11]. This procedure induces a fine microstructure, necessary condition in the alloy to present the superplastic behavior. Such microstructure results from a β-phase transformation that occurs in the Zn–Al system, Fig. 9: β (triclinic)→η (hcp) phase+R (rhombohedral). Additionally, the R phase splits in two phases: R (rhombohedral)→η (hcp)+α (fcc) [46]. This transformation is in agreement with the observed Zn- and Al-rich phases with the respectively clear and dark EBS-contrast in the SEM-image.

On the other hand, the large homogeneous microstructure of alternated Zn and Al sheets of 200 nm size, produced in this work, was perhaps due to the more efficient heat dissipation by the quenching in acetone at 0 °C, in comparison to that in ice water at 15 °C used to produce this microstructure type in the same alloy [11].

5.3. Compressive behavior

The Young modulus measured in the elaborated solid Zn22Al2Cu alloy (90 GPa) is lower than those obtained for the same alloy, but processed by semi-continuous casting (197.5 GPa) [47] and in permanent mold (110–130 GPa) [48–50]. While its yield stress (363 MPa and 390 MPa, for the casting and fine microstructures, respectively) lies between the yield stresses for this alloy produced in a permanent mold (300 MPa) and by semi-continuous casting (395 MPa).

It is clear from Fig. 8 that the compressive behavior depends on both the composite density and the microstructure type. Further, those composites with fine matrix microstructure have a behavior with a more regular variation schema, than those with a casting matrix microstructure, when the density varies. To illustrate this and to define some related parameters, in Fig. 10 the compressive stress–strain curve of the composite with fine microstructure and 2.7936 g/cm^3 is shown alone, as a model for subsequent discussions. All compressive stress–strain curves exhibit in general this model behavior, i.e., three characteristic regions, namely a linear elastic response, a plastic deformation region and a sudden increase of stress; the first two regions are separated by a maximum stress. This behavior is similar to that attributed to metal foams, which have empty cells or trapped gas instead of solid glass spheres [51]. At the elastic region, where flexion or bending of cells walls take place up to a maximum stress, named collapse stress value, σ_{col}, when matrix collapses and the cell walls undergo a plastic deformation, torsion or rupture. This behavior extends across the sample as bands and slight stress variations occur around a central value, which is associated to the stress plateau, identified by σ_p in the compression curve. Finally, a sudden stress increase is required to produce a small strain because foams begin their densification by crushing cells.

Fig. 11 shows the curves of elastic modulus for the composites processed, E_C, with casting and fine microstructures, respect to the elastic modulus of matrix, E_m, as a function of the relative density, (ρ_c/ρ_m). Using the least-squares method to fit the experimental data E_c/E_m vs ρ_c/ρ_m to an expression like $y=Cx^a$ as in Eq. 4, it was found: $C=6.58$, $a=4.6$, and R^2 (determination coefficient)$=0.89$ for the casting microstructure, $C=2.15$, $a=2.35$ and $R^2=0.26$ for the fine microstructure.

In Figs. 12 and 13 the relative maximum stress and relative plateau stress are plotted in respect to the yield stress of the matrix, σ_{max}/σ_{ym} and σ_p/σ_{ym}, respectively, as a function of the relative density, ρ_c/ρ_m, for the composites with casting and fine microstructures. The experimental data σ_{max}/σ_{ym} and σ_p/σ_{ym} vs ρ_c/ρ_m were fitted by the least-squares method as before, obtaining the following parameters: $C=3.26$, $a=2.85$, $R^2=0.30$ and $C=1.26$, $a=1.42$, $R^2=0.33$ for the relative σ_{max} for composites with casting and fine microstructures, respectively; $C=1.12$, $a=1.45$, $R^2=0.07$ and $C=1.04$, $a=1.92$, $R^2=0.15$ for relative plateau stress of composites with casting and fine microstructures, respectively.

Therefore, although composites exhibit very similar stress–strain-compression curves to those reported for foams tested under compression, the characteristic parameters of these curves do not vary with the density, as is stated by Eqs. (4) and (5) of Ashby.

The values of the upper and lower limits of the elastic modulus ratio, E_{UL}/E_m and E_{LL}/E_m, respectively, were calculated by introducing the spheres volume fraction, X_s of Table 1, in Eqs. (2) and (3). It can be observed from Fig. 11, that these values are overestimated in respect of the measured elastic modulus ratios.

Two stress values are used to define the first stress fall of the stress–strain curves in Fig. 8, namely the upper and lower yielding points (UYP and LYP), see Fig. 10. Therefore, the difference

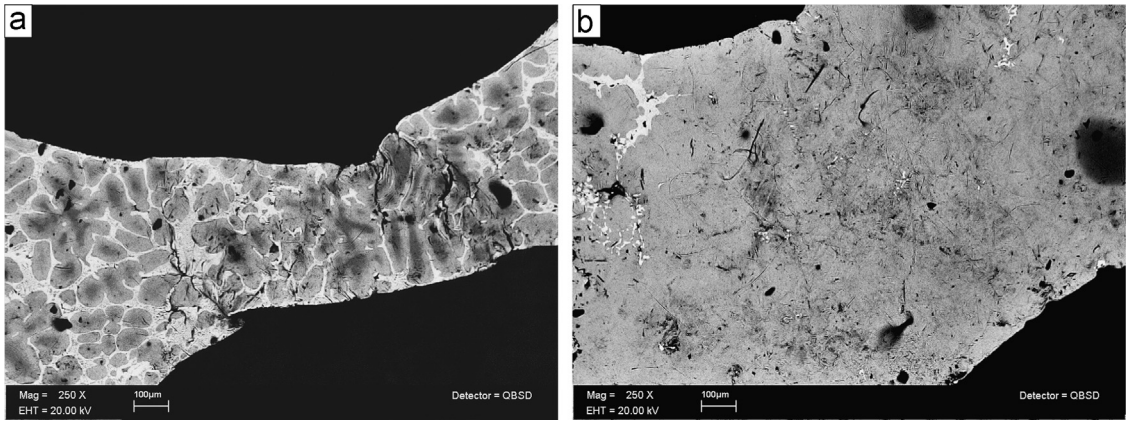

Fig. 17. BSE–SEM-image of cell walls in the composite samples after the third stage of deformation: (a) casting microstructure and (b) fine microstructure in matrix. Note that the fissures take place through the Zn-rich phase (η).

between these two values is a measure of the stress fall after the spheres rupture. At Fig. 14, they are graphed as a function of the relative density, and it is evident that the stress fall is always more pronounced for composites with fine microstructure in the matrix. This experimental evidence could be interpreted as if such fine-grained microstructure transfers easily the stress to the spheres and it diminishes drastically for this microstructure, as soon as the spheres break.

In order to support this interpretation, samples with both matrix microstructures, were tested stage by stage under compression, at the same strain rate employed for the continuous compression experiments. In Figs. 15 and 16 are shown images series of samples with the casting and fine microstructures, respectively, deformed by stages. The stress and deformation reached in each step are pointed out below the corresponding image. It is evident from both series of images that most of the spherical skullcaps were broken at the end of the first deformation stage. This event can be related to the first stress fall in the stress–strain curves, Fig. 8, of the continuously deformed samples.

Compression by stages also allowed to observe, that the cells walls were deformed after the spheres broke, then the cavities at the samples top crushed together because the deformation is concentrated there. This process was sequentially repeated along the samples, at subsequent deformation stages. Fig. 17 shows the effects produced after the third stage of deformation at both casting and fine microstructures. Note that fisures take place at the Zn-rich interdendritic phase. Therefore, the materials studied behave as foams, after rupture of glass-caps.

In Table 2, it is compared the energy absorption capacity and the maximum compressive stress of the composites studied in this work, with similar materials reported elsewhere. It is interesting to note that all the maximum compressive strength values reported are lower than those obtained in this work. Moreover, our energy absorption capacity values are higher than the reported ones, except for those values obtained with higher densities in syntactic foam composites.

Table 2
Important data obtained in the present work compared with reported ones.

Matrix	Material type	Microstructure in matrix	Energy absorption capacity (MJ/m^3)	Compressive strength (MPa)	Densities ratio	Process	Reference
Zn22Al2Cu	Foam composites with glass solid spheres	Casting	31.22–64.11[a]	122.4–262.8[c]	0.4978–0.5782	Alloy melting, spheres immersion, cooling of slurry in air.	Present work
		Fine-grained	32.29–47.28[a]	160.9–230.9[c]			
Zn22Al	Foam Composites with SiC particles	Casting	0.96–1.18[a]	~3.5–4.64[c]	0.177–0.186	Stir-casting	[36]
Zn22Al with 1.0Cu and 0.03Mg	Foams with open cells	Casting	3–7.5[a]	4.7–20[d]	0.279–0.396	Replication with NaCl preforms	[37]
Zn22Al	Syntactic foam composites with Ni-coated fly ash microballoons	Fine-grained	55–133[b]	75–200[c]	0.623–0.962	Stir-casting	[40]

[a] $\varepsilon = 0.34$.
[b] $\dot{\varepsilon} = 0.60$ and $8.3 \times 10^{-4}\ s^{-1}$ strain rate.
[c] First stress maximum.
[d] Collapse stress.

6. Conclusions

The casting matrix microstructure was found to be integrated by dendrites and an interdendritic component. By increasing density, the Zn rich interdendritic component diminished substantially, and at the same time, Al rich centers fenced by intermediated Zn–Al regions increased. The thermally induced matrix microstructure showed fine grains, 0.2 μm in mean size, being bigger, 1 μm, near to the spheres; these features did not change with the density.

All composites showed a linear elastic behavior at low strains, reaching their maximum stress at relative high values in the ranges 122.4–262.8 MPa and 160.9–230.9 MPa for composites with casting and fine matrix microstructures, respectively. Thereafter, a stress fall took place because the spheres broke, followed by an important plastic deformation at nearly constant stress. The mean value of the plateau stress changed with the composite density between 90–210 MPa and 70–130 MPa for composites with casting and fine matrix microstructures, respectively. Finally, the composites required a significant increase in stress to get an additional deformation. This mechanical behavior under compressive stress is similar to that exhibit by metallic foams. Elastic modulus, maximum stress and plateau stress were found to change with density in different way as Ashby equations predictions.

As a main conclusion, we can say that the solid glass spheres – Zn22Al2Cu composites studied in this work, behave mechanically under compression like a solid foam.

References

[1] Y. Zhang, X. Zeng, L. Yang, K. Sun, Z. Song, Philos. Mag. Lett. 93 (6) (2013) 322–330.
[2] M.A.M. Arif, M.Z. Omar, N. Muhamad, J. Syarif, P. Kapranos, J. Mater. Sci. Technol. 29 (8) (2013) 765–774.
[3] W. Xiao, et al., J. Univ. Sci. Technol. Beijing 33 (10) (2011) 1248–1252.
[4] A.E. Ares, C.E. Schvezov, J. Cryst. Growth 318 (1) (2011) 59–65.
[5] Y. Shuqing, et al., J. Mater. Sci. Technol. 26 (7) (2010) 648–652.
[6] J. Joong, et al., J. Alloy. Compd. 434–435 (2007) 311–314.
[7] Y. Li, W. Xu, D. Ma, Y.P. Feng, Philos. Mag. Lett. 80 (7) (2000) 467–475.
[8] T. Kokubo, G. Itoh, Y. Motohashi, Mater. Sci. Forum 551–552 (2007) 153–156.
[9] Z.Q. Shi, Y.H. Liu, S.C. Li, J. Mater. Eng. 6 (2004) 33–36.
[10] S.R. Casolco, J. Negrete-Sanchez, G. Torres-Villaseñor, Mater. Charact. 51 (1) (2003) 63–67.
[11] M. Ramos, E. Martinez, G. Torres, J. Mater. Sci. 47 (2012) 6206–6212.
[12] M. Kawasaki, T.G. Langdon, J. Mater. Sci. 48 (2013) 4730–4741.
[13] R. Mojaver, H.R. Shahverdi, Wear 271 (11–12) (2011) 2899–2908.
[14] Y. Chih-Fu, P. Jiun-Hung, L. Te-Hao, J. Alloy. Compd. 468 (1–2) (2009) 230–236.
[15] E.M. Da Costa, et al., J. Alloy. Compd. 488 (1) (2009) 89–99.
[16] H.J. Dorantes-Rosales, V.M. López-Hirata, R. Esquivel-González, J.L. González-Velazquez, J. Moreno-Palmerin, A. Torres-Castillo, Met. Mater. Int. 18 (3) (2012) 385–390.
[17] Y.Z. Zhao, Q. Gao, Y.C. Liu, Acta Metall. Sin. (Engl. Lett.) 19 (3) (2006) 228–234.
[18] D.B. Miracle, Sci. Technol. 65 (2005) 2526–2540.
[19] K.U. Kainer, Metal Matrix Composites: Custom-made Materials for Automotive and Aerospace Engineering, Wiley-VCH, Hoboken, New Jersey, 2006.
[20] M.F. Ashby, L. Tianjin, Sci. China (Ser. B) 46 (6) (2003) 521–532.
[21] J.S. Kim, J. Kaneko, M. Sugamata, J. Jpn. Inst. Met. 55 (9) (1991) 986–993.
[22] J.S. Kim, M. Sugamata, J. Kaneko, J. Jpn. Inst. Met. 55 (9) (1991) 994–1001.
[23] X. Xu, W. Wang, L. Cai, J. Mater. Sci. Technol. 20 (2) (2004) 172–174.
[24] P. Zhu, W.Y. Yeung, G.B. Heness, J. Duggan, Mater. Sci. Forum 475–479 (2005) 979–984.
[25] Y. Xun, F.A. Mohamed, Philos. Mag. 85 (24) (2005) 2767–2785.
[26] E. Martinez-Flores, J. Negrete, G.T. Villaseñor, Mater. Des. 24 (4) (2003) 281–286.
[27] J.A. Aragón, J.R. Miranda, Rev. Mex. Fis. 51 (4) (2005) 356–364.
[28] G.R. Goldak, J.G. Parr, J. Inst. Met. 92 (1963) 230–233.
[29] E. Martínez-Flores, G. Torres-Villaseñor, Hibrid materials based on Zn–Al alloys, in: J. Cuppoletti (Ed.), Metal, Ceramic and Polymeric Composites for Various Uses, InTech, Florida, US, 2011, pp. 149–170 (Chapter 7).
[30] J.A. Aragón, J.R. Miranda, I. Hilerio, D. Muñoz, R. Hernández, V. Cortés, et al., Rev. Mex. Fis. 53 (2) (2007) 105–113.
[31] J. Liu, et al., Mater. Lett. 62 (2008) 683–685.
[32] J. Liu, et al., J. Alloy. Compd. 476 (2009) 466–469.
[33] K. Sekido, K. Kitazono, Mater. Sci. Forum 735 (2013) 73–78.
[34] J. Liu, et al., Mater. Lett. 62 (2008) 3636–3638.
[35] S. Yu, et al., Mater. Sci. Eng. A 457 (2007) 325–328.
[36] J. Liu, et al., J. Alloy. Compd. 476 (2009) 220–225.
[37] S. Yu, et al., Mater. Des. 30 (2009) 87–90.
[38] S.R. Casolco, et al., Mater. Sci. Eng. A 471 (2007) 28–33.
[39] K. Kitazono, Y. Takiguchi, Scr. Mater. 55 (2006) 51–54.
[40] A. Daoud, Mater. Sci. Eng. A. 488 (2008) 281–295.
[41] M.F. Ashby, Metall. Trans. A 14 (1983) 1755–1769.
[42] A. Flores-Ramos, et al., Rev. Metal. 50 (4) (2014) e026, http://dx.doi.org/10.3989/revmetalm.026.
[43] Y.H. Zhu, E. Orozco, Metall. Mater. Trans. 26A (1995) 2611–2615.
[44] J. Negrete, A. Torres, G. Torres-Villaseñor, J. Mater. Sci. Lett. 14 (1995) 1092–1094.
[45] A.A. Presnyakov, Y.A. Gorban, V.V. Chernyakova, Russ. J. Phys. Chem. 35 (1961) 623–633.
[46] A. Sandoval-Jimenez, J. Negrete, G. Torres-Villaseñor, Mater. Charact. 61 (2010) 1286–1289.
[47] J. Hinojosa, J. Montemayor, G. Torres, Rev. Mex. Fis. 37 (1) (1991) 104–114.
[48] G. Torres, M. Lopez, Natl. Acad. Sci. (1980) 238–240.
[49] G. Torres, Rev. Mex. Fis. 3 (1985) 489–501.
[50] G. Torres, J. Hinojosa, Moldeo Fundic. 51 (1987) 33.
[51] H.P. Degischer, B. Kriszt, Handbook of Cellular Metals: Production, Processing, Applications, Wiley-VCH, Hoboken, New Jersey (2002), p. 181–182.